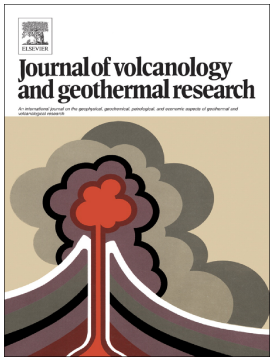

Hydrovolcanic ash emission between August 14 and 24, 2015 at Cotopaxi volcano (Ecuador): Characterization and eruption mechanisms

Liliana Troncoso, Jorge Bustillos, Jorge E. Romero, Alicia Guevara, Janina Carrillo, Estefano Montalvo, Tatiana Izquierdo

PII: S0377-0273(16)30269-4
DOI: doi: 10.1016/j.jvolgeores.2017.05.032
Reference: VOLGEO 6117

To appear in: *Journal of Volcanology and Geothermal Research*

Received date: 18 August 2016
Revised date: 14 May 2017
Accepted date: 30 May 2017

Please cite this article as: Liliana Troncoso, Jorge Bustillos, Jorge E. Romero, Alicia Guevara, Janina Carrillo, Estefano Montalvo, Tatiana Izquierdo , Hydrovolcanic ash emission between August 14 and 24, 2015 at Cotopaxi volcano (Ecuador): Characterization and eruption mechanisms, *Journal of Volcanology and Geothermal Research* (2017), doi: 10.1016/j.jvolgeores.2017.05.032

Hydrovolcanic ash emission between August 14 and 24, 2015 at Cotopaxi Volcano (Ecuador): Characterization and eruption mechanisms

Liliana Troncoso[1]*, Jorge Bustillos[1], Jorge E. Romero[2], Alicia Guevara[3], Janina Carrillo[1], Estefano Montalvo[1], Tatiana Izquierdo[2]

[1] Facultad de Geología, Minas, Petróleos y Ambiental, Carrera de Ingeniería en Geología. Universidad Central del Ecuador - Casilla 872 A, Quito, Ecuador.

[2] Departamento de Geología, Universidad de Atacama - Copayapu 485, Copiapó, Chile

[3] Departamento de Metalurgia Extractiva, Escuela Politécnica Nacional - Ladrón Guevara E11-253, Quito, Ecuador.

* Contact e-mail: lptroncoso@uce.edu.ec

Abstract

Cotopaxi is an active, hazardous and ice-covered stratovolcano 60 km southeast of Quito, (Ecuador) whose last major eruption occurred in 1877. During 2001-2002, volcanic unrest characterized by volcanic seismicity and deformation ended without eruptive activity. On April 2015, a new increase of seismicity, SO_2 emissions, thermal anomalies and edifice deformation, evolved into the onset of a new eruptive cycle, beginning August 14. We sampled and measured the ash fall deposits to the west of Cotopaxi between August 14 and 24, 2015. The ash collected was analyzed using grain size, X-Ray fluorescence, X-Ray diffraction and scanning electron microscope (SEM-EDS), revealing the eruptive products to be compound of dense fragments (mostly lithics), diverse types of scoria, pumice, free fractured crystals, volcanic glass and aggregates. Most of hydrothermal alteration is observed during the initial stage of the eruption (14-15 August; including Cu oxides and Fe minerals in the lithics). The glassy particles were blocky morphology, and textural changes were recognized over 10 days of eruption, varying from null or low vesicularity to low-to-moderate vesicularity, occasionally exhibiting molten or subrounded textures. The bulk ash has a basaltic-andesitic composition (~55.67 wt. % of SiO_2), while clusters of selected particles (likely juvenile) analyzed through SEM + EDS reveal dacitic composition (65.67 and 65.8 wt. % SiO_2). Plagioclase, clinopyroxene and orthopyroxene are the main minerals present, with accessory anhydrite, melanterite and pyrite (these typically observed during the initial stage of eruption). These variations in addition to the geophysical background, led us to interpret this eruption as the result of the volcano's hydrothermal system disruption due to a shallow, low-volume magma input, which initially evolved into phreatic activity at surface level. Further activity up to 24 August was triggered by the indirect interaction between magma and the depleted hydrothermal system, generating a magmatic-hydrothermal eruption. The issue is important for evaluating unrest periods at active stratovolcanoes, and the impact of their initial, low-volume ash falls in neighboring communities.

Keywords: ash fall deposit, eruption mechanism, juvenile content, Cotopaxi Volcano.

1. Introduction

All kinds of volcanism involving magma-water interaction, explosive or nonexplosive, surface or subsurface, subaerial or submarine, are currently grouped as "hydrovolcanism" (Zimanowsky et al., 2015). From these, Phreatic explosions are caused by heating and flashing of water produced when magma comes into contact with water but only country rock or overburden is ejected, without fresh juvenile magmatic material (Browne and Lawless, 2001). When magmatic material is injected into a pre-existing convective hydrothermal system causes a heat pulse that triggers magmatic-hydrothermal eruptions, thus the energy responsible for the eruption is derived from the hydrothermal system itself, but the magmatic input has an essential triggering role and fresh juvenile magmatic material may or may not be identifiable (Lawless et al., 1997). Most intensive type of magma-water interaction, occurring when a mixture of magma and water evolves into a thermohydraulic explosion is known as phreatomagmatic eruption (Zimanowsky et al., 2015).
When fresh juvenile magma content is scarce or not clearly distinguished within samples, difficulties to differentiate from phreatic and phreatomagmatic eruptions are reported (e.g. Pardo et al., 2012). For example, the misunderstood of older fallout deposits by fresh juvenile components left strong impacts on hazard evaluation and risk manegement during La Soufriere 1975-77 phreatic activity (e.g. Hincks et al., 2014). Thus, an appropriate identification of fresh juvenile magma content may be crucial for distinguishing between low-level volcanic restlessness from activity that presages a larger eruption (eg. Cashman and Hoblitt, 2004). For these cases, studying ash by grain size analysis and microscopic investigation provides valuable information on the eruptive mechanism (Dellino and Kyriakopoulos, 2003).A typical eruption product from hydrovolcanism is tephra. Tephra dispersion is one of the major volcanic hazards related to explosive eruptions (Kawabata et al., 2013), with adverse affects to agriculture, water quality, critical infrastructure, transportation and human health (e.g. Horwell and Baxter, 2006; Wilson et al., 2012). The quantification of tephra volumes is necessary in order to determine magnitude, dynamics and hazard at explosive volcanoes (Bonadonna and Costa, 2012). However, assessing the threat of tephra fall depends on additional factors, including event duration and timing, grain size, mineralogy and soluble acidic salt content (Magill et al., 2013).

Cotopaxi Volcano (Ecuador; Fig.1) is an active ice-covered stratovolcano located 60 km southeast of Quito (~2.234.000 inhabitants) at an elevation of 5,987 m. Within the 21st century, the volcano experienced two increases in its seismic activity in 2001 and 2015 (Molina et al., 2008; IGEPN, 2015a), whose the last unrest in 2015 also produced low-energy, locally-distributed ash emissions (Fig. 2). Analyses of the Cotopaxi 2015 ash emissions report both juvenile material produced by hydromagmatic eruptions (e.g. Gaunt et al., 2016) and no juvenile material ejected by phreatic explosions (e.g. Vaca et al., 2015; Bernard et al., 2016). As a result, both eruption mechanism and potential volcanic hazard remain unclear. This work seeks to better explain the eruption mechanism during the August 14, 15 and 24, 2015 ash emissions of Cotopaxi volcano. The thickness, grain size, lithology, texture, geochemistry and mineralogy are all measured. These characteristics are then analyzed in terms of eruptive mechanism, which in turn are used to characterize the volcanic hazard.

2. Cotopaxi volcano and its reawakening in 2015

2.1 Volcanism and historical activity of Cotopaxi volcano

Cotopaxi volcano has erupted a total DRE volume of 28.54 km^3 during the last 0.5 Ma (Hall and Mothes, 2008), with frequent eruptions over the last 2 ky (one event every ~117 years, on average). Activity included lava effusion to explosive activity with Strombolian and Plinian styles, whose higher columns (28-39 km) deposited bulk tephra volumes ranging from 0.1 to 0.65 km^3 (VEI 3-4) (Barberi et al.,1995). In addition, the stratigraphic study of the post-12^{th}-century eruptive products reveals 21 continuous tephra falls with peak mass discharge rates from 1.1×10^7 to 9.3×10^7 kg s^{-1} associated with moderate magma volumes ($1.1\times10^{10} – 6.0\times10^{11}$ kg; Pistolesi et al., 2011). Cotopaxi has experienced at least 13 andesitic eruptions since 1534 corresponding to five eruptive cycles: 1532-1534, 1742-1744, 1766-1768, 1853-1854, and 1877-1880 (Hall and Mothes, 2008, Wolf, 1878). These historical eruptions also produced rapid snow/ice melting of the summit ice cap, resulting in lahars that traveled downstream hundreds of kilometers from their source and caused major damage to the settlements around the volcano (Pistolesi, 2008). Cotopaxi is currently covered by 20 km^2 of snow and ice, with a volume of 1.0 km^3 (Mothes et al., 1998).

According to Pistolesi et al. (2011) the volcanic reactivations reported in 1904, 1906, and 1912, consisted of minor explosions that affected only the crater area. More recent unrest at Cotopaxi occurred in 1975-1976 and 2001–2002 and were characterized by an increase in fumarolic activity, elevated seismicity and edifice deformation that continues today (Constantinescu et al., 2015). Cotopaxi has been monitored by the Instituto Geofísico (Escuela Politécnica Nacional, IGEPN) since 1983, providing detailed information on volcano seismicity, deformation, geochemistry and degassing. From 1989 to 1997 the seismic activity below Cotopaxi was characterized by long-period (LP) and volcano-tectonic (VT) events between 2 km and 8 km depth below the volcano, which were interpreted as the interaction of meteoric water and hot shallow material (Ruiz et al., 1998). Renewed seismic activity began in January 2001 with an increased number of LP events and a swarm of VT earthquakes in November 2001 followed by very-long-period (VLP) events in late June 2002, being interpreted as magma input, gas release and resonance of this gas in a crack above the magma system by Molina et al. (2008). Hickey et al. (2015) has discussed this unrest as a consequence of fluid migration produced by a low magma supply rate, from the SW into the NE along NNE-SSW trending faults, causing the seismicity due to mass transport and excess pore pressures, with a volume change of ~20 x 10^6 m^3.

2.2 The August 2015 eruptions

In 2015, the IGEPN monitoring network consisted of 11 broadband and 5 short period seismometers, 4 scanning DOAS, 1 infrared and 5 visible cameras, 7 DGPS, 5 tilt-meters, 11 AFM (lahar detectors) and a network of ash-meters (Hidalgo et al., 2016). According to the IGEPN, the Cotopaxi volcano experienced increased seismic activity on April 2015 (if compared to the base level of the period 1989-2014) of VT, LP, VLP and tremor events together with an increase in the SO_2 emissions (from the normal 0,5 kt/day to ~3,0 kt/day) and a small inflation of 150 μrad in the northeast flank as measured with a tilt-meter after 21 May (IGEPN, 2015a, b; Arias et al., 2015; Mothes et al., 2016). According to Gaunt et al (2016), since the beginning of April 2015, a constant increase of LP seismicity was recorded up to the end of May, when these

events reached a maximum of about 160 events per day. LP seismicity decreased by half July with many oscillations observed up to August. The seismicity originated at a depth of 2-3 km beneath the volcano summit, while a series of inflation-deflation periods suggest a deeper intrusion initiating at 10-11 km depth, ascending to 7-8 km depth by May 2015 with variable volumes of about 4-31 x 10^6 m^3 (Arias et al., 2015). A seismic swarm started on August 13 at 22.21 UTC below the volcano and persisted for almost 45 minutes with a maximum magnitude event of 2.7 Ml (IGEPN, 2015c). On August 14, LP events increased up to >260 per day and VT events also increased to >35 per day preceding a series of explosions. Two discrete explosions occurred at 09.02 and 09.07 UTC, the first of which produced a shockwave of 6 Pascal in amplitude and caused ash fallout at towns of Machachi, Amaguaña, Boliche, Tambillo and south of Quito (IGEPN, 2015c, d). According to reports from residents of Puichi and Machachi (ca. 24 km NW from the crater), the ash fall started at 09.30 UTC and persisted until 11.30 UTC and was accompanied by sulfur odor. Later, at 15.25 UTC, a third explosion produced an ash-loaded convective column (e.g. Tvcolor36, 2015) of 6-8 km in height above the crater level (acl), and was associated with ash fallout towards the NW and SW of the volcano. It was followed by two other explosions at 18.45 UTC and 19.29 UTC (IGEPN, 2015d). A peak of SO_2 emission rate of 24 kt/day accompanied these explosions, being followed by the instrumental detection of BrO and HCl, plus increasing CO_2/SO_2 ratio from 1 to 2.5, indicating a shallow magmatic origin of the gas (IGEPN, 2015e; Hidalgo et al., 2016). Small ash emissions with weak eruption columns elevated at 0.2-2 km acl were almost permanent during the period August 15-24 (Fig. 2A; e.g. Paredes, 2015), and in some cases they were interrupted by vapor and gas-laden emissions (e.g. Chancusig, 2015), with relative calm lasting few hours (without ash emissions). A small explosion was also observed on August 20. In this period, the seismicity was characterized by the occurrence of LP, VLP, VT (following an increasing trend) and emission tremor events, all originating 1 to 4 km beneath the volcano. Towards the end of August, new thermal anomalies (13.5 to 16.3 °C) were detected at the N flank glaciers, being associated to source areas with fumarolic activity together with the formation of narrow streams of water in September 2015 (Ramón et al., 2016). Small GPS and tilt changes leveled off in November 2015 (Mothes et al., 2016), and surface manifestations and other monitored parameters decreased from this date (Hidalgo et al., 2016). The ash fallout caused respiratory and eye problems in the inhabitants of towns around Cotopaxi volcano (e.g. Machachi), and also impacted to livestock, agriculture and humman activities (Fig. 2B; e.g. Afpes, 2015).

The initial work of Vaca et al. (2016) categorically excluded the presence of juvenile material and concluded that the 2015 eruption was a minor sporadic event (phreatic?). Bernard et al. (2016) suggested that the pre-eruptive tremor was generated by the boiling of the hydrothermal system due to a magmatic intrusion and consequently produced hydromagmatic fragmentation, followed by the drying out or insulation of the hydrothermal system around the intrusion and the cleaning of the volcano conduit. By other hand, Gaunt et al. (2016) described the ash within the first week of eruption as rich in lithics, hydrothermally altered grains, oxidized lithic material and juvenile glassy grains. The initial explosions and emission phase over the first two days are therefore interpreted as hydro-magmatic when the rising magma served primarily as a heat source that disturbed the fragile equilibrium of the hydrothermal system. The subsequent activity, characterized by highest emission rate, ash with lower amount of lithics and

hydrothermally altered rocks, plus increasing juvenile material with higher amount of microlites was interpreted as the repetitive shallow plugging of the conduit.

3. Methods and materials

3.1 Dispersion of ash plumes

We describe the plume dispersion based on Geostationary Operational Environmental Satellite images (GOES-13; http://cimss.ssec.wisc.edu/goes/blog/archives/19249) of the explosions on August 14 with the plume top temperatures reported there. We estimated the column heights in the base of the meteorological observations of August 14 given by the Guayaquil city radiosonde data (code 84203) from the Wyoming University (http://weather.uwyo.edu). The ash emissions of the following days were observed through the Earth Observing System Data and Information System (EOSDIS; https://worldview.earthdata.nasa.gov/) and via ASTER satellite images (http://ava.jpl.nasa.gov/). To compare these ash dispersion patterns, the wind Reanalysis code (Palma, 2013) was applied in order to determine the statistical wind directions over Cotopaxi from 1999 to 2011. We selected different altitude datasets (7, 10 and 15 km height above the sea level, asl) which correspond to the heights of the eruption plumes within the studied period. The analysis gathered 2728 wind direction tendencies corresponding to August.

3.2 Ash sampling strategy

Field sampling of ash fallout (Fig. 3) was carried out on August 14 and 15 after the first and second explosions at Machachi (Mch) and Aloasí (Alo) towns, and on August 24 we sampled and measured additional ash blankets at Mulaló (Mul), San Ramón (SR), San Agustín de Callo (SAC), Lasso (Lss) and in Cotopaxi National Park (CNP). In many cases, the cemeteries of those towns around Cotopaxi volcano were selected as sampling sites due to the excellent preservation of ash (Table 1) whereas in other cases we observed thin, non-uniform deposits (Fig. 3). Thus, we applied a correction factor (Cf) for the thickness measurements on the basis of the % of covered surface (Cf; Fig. 2). For example, for a Cf ~30% ash-covered surface of 1 m^2 in area (A) and ~0.5 mm in thickness (T), the resulting volume (V) at the collection point is given by $V = T\ x\ A\ x\ Cf$, where Cf = 0.3. Due to the scarce field data, drawing of deposit isopachs was not possible. Ash samples were collected in areas of 1 m^2 at selected sites that correspond to plane areas without evident reworking of the ash (Fig. 3).

3.3 Ash characterization

The ash samples were dried at 40° C for 48 h and weighed afterwards; deposit density calculations were performed using these dry weights. In order to obtain grain size distributions, dry mechanic sieving was performed on each sample in the range 1.5 to 5.0 Φ, at regular steeps of 0.5 Φ ($\Phi=-\log_2 D/D_0$, with D is the particle diameter and D_0 a reference diameter as 1 mm). There has been demonstrated that wet sieving results in a more uniform grain size distribution and a shift in particle size towards the <63 μm fraction (Robertson et al., 1984). However, some natural volcanic particles such as aggregates tend to disaggregate on impact through a water column (Brown et al., 2012).

For this reason, we selected the dry method in order to search for aggregates. For sample classification, we applied the *Gradistat* package (Blott and Pye, 2001) statistical parameters of Inman (1952) and Folk and Ward (1957).

The components were optically analyzed with a binocular amplifying glass at 1.5 Φ grain size class from >100 particles and the different particle types were quantified by modal % abundance. The modal % abundance of each particle type could vary at different grain size classes, with effects in the componentry description. For comparison, Gaunt et al. (2016) analyzed a similar grain size class (1.0-1.5 Φ), after a manual dry sieving. Scanning electron microscope-energy dispersive spectrometry (SEM-EDS) was used for the characterization of ash morphology and also for the surface geochemical mapping of two clusters of selected grains (suspected to be juvenile >3.3 Φ) from both 14 and 24 August samples. The X-ray intensities given by the EDS spectrometer were converted to wt. % oxides. These analyses were performed at the Departamento de Metalurgia Extractiva at the Escuela Politécnica Nacional (DEMEX-EPN) using a Tescan-Vega (Bruker) instrument, which was operated at 15.0 kV and a work distance (WD) between 18 and 23 mm.

The chemical analysis (major elements) of the ash was carried out using a X-Ray fluorescence (XRF) S8 Tiger instrument, and the data was managed with the software Spectra Plus. The determination of minerals in ash was obtained with a X-Ray diffraction (XDR) D8 Advance instrument, and the software Diffract Plus (EVA and TOPAS) for the quantification and semi-quantification of minerals (Table 4). These phases were compared to the XRD spectrums of the International Center of Diffraction Data (ICDD) database.

4. The August 14-24 (2015) fallout deposits

4.1 Dispersion of the ash plumes

The most frequent wind blowing direction at Cotopaxi volcano at an altitude of 7 to 10 km asl is W-SW (Fig. 4A). In contrast, more variability is observed at higher altitude (15 km) were the wind blows in multiple directions (from NE to ESE and from N to W; Fig. 4A). This is in agreement with the plumes observed during the August 2015 eruption, from whose the lower ones were dispersed W-WSW and the higher ones drifted NW and ESW (Fig. 4B). Using the satellite GOES-13 imagery, it was possible to better reconstruct these wind tendencies. The eruption plume was initially observed by 14 August at 09.28 UTC being dispersed to the SE (Fig. 5A), and appeared completely detached from the source at 10.58 UTC (Fig. 5B) and completely diluted at 12.58 UTC. A new plume, associated to the third explosion was observed at 15.45 UTC (Fig. 5C) and it was dispersed towards the NW. At 16.28 UTC, the plume was partially diluted into the atmosphere (Fig. 5D) and a second smaller plume was drifting to the W-SW. The temperature of the third explosion plume was near -53 °C, what suggests an altitude of ~8.7 km asl. Even when at 17.15 UTC the plume seems to continue expanding and a detaching from the source area is not evident, it is more diluted and there was no longer ash supply into the plume, indicating the end of the eruptive activity. The plume was unquestionably detached from its source at 18.15 UTC. Another large explosion occurred at approximately 18.45 UTC and persisted until 19.45 UTC. In contrast to the

preceding explosions, this plume was dispersed toward the E and NE reaching a cloud top with a temperature near to -72.7 °C, what corresponds to 13 km in altitude. During the following days, the ash drifted mainly to the W (between 249° and 284° azimuth; Fig. 3E) and the plumes had lengths varying from 20 to 280 km.

4.2 Distribution of ash fallouts

Due to the difficulty of mapping very thin ash blankets (<1 mm; Fig. 3), which are easily reworked, and unsafe conditions for measuring proximal outcrops, only four data points were measured between 12.30 and 14.00 UTC on August 14, and four other data points for the explosions that occurred at 15.25, 18.45 and 19.29 UTC. These events were distributed toward the northwest of the volcano. On August 24, six data points of ash thickness were measured towards the W of the volcano, with thicknesses varying from 0.5 to 2.5 cm (Table 1). From four dry apparent density (ρ) measurements, we obtained an average ρ=66.3 kg/m^3 for the ash. However, this value could be not realistic due to the lack of proximal (<15 km downwind) ρ data, and after interpolating this value using relations of ρ versus distance from the vent, we assumed a minimum deposit ρ of ~100 kg/m^3.

4.3 Grain size analysis

The grain size analyses carried out to the August 14-24 2015 samples of Cotopaxi ash are summarized in Table 2 and Fig. 6. All the samples are compound, with dominant fractions (median and mode) varying from coarse to fine ash (1.0 to 3.0 Φ). Samples collected on August 14 at Machachi and Aloasí cemeteries (Fig. 6A and 6B) are poorly sorted (σ=1.019-1.155 Φ) and show fine to very fine skewned (S_K= 0.390-0.189 Φ) and trimodal grain size distributions (Table 2). On the other hand, sample 3, collected on August 15 at Aloasí shows a bimodal, moderately sorted (σ=0.67 Φ) grain size distribution (Fig. 6C; Table 2). Finally, samples from August 24 (Fig. 4D to 4I) mostly present a bimodal distribution and are moderately well sorted (σ= 0.60-0.65 Φ) with skewness varying from -0.37 to 0.14 Φ, with the exception of the samples collected at Aloasí and Lasso (Fig. 6E and 6H, respectively; Table 2), which are unimodal and well to very well sorted (σ= 0.22-0.34 Φ). In all the samples, the cumulative finest fraction of ash (>5 Φ) vary from 5.7 to 96.9 wt. % (Fig. 5), with an average of 42.7 wt. % and standard deviation to 29.3 wt. %.

In general terms, trimodal grain size distributions are only seen during the initial phase of activity (August 14, samples 1 and 2), while at August 24 there is a sample with unimodal distribution at Cementerio Aloasí. During August 24, grain size distributions were mostly bimodal (ca. 83 %) with only one unimodal sample.

4.4 Lithology

The lithology of the samples is summarized in Fig. 7 . Sample 2, collected on August 14 at Aloasí cemetery is dominated by: 1) a 30 % of dense, unaltered, porphyritic, gray and subangular fragments, and contains plagioclase (pl), piroxene (px) and pirite; 2) black scoria (20 %) characterized by a subangular morphology and high-vesicularity with spherical vesicles; 3) aggregates (20 %) with grey, red or white color and variable morphology from subangular to subrounded, in some cases elongated or planar. The reddish scoria (hydrothermally altered scoria), pumice and volcanic glass shards

represent 10 % of the sample, respectively. Reddish scoria is subangular to subplanar, with moderate to high vesicularity. Pumices, in contrast, show very low vesicularity with subangular vesicles that present planar surfaces. Volcanic glass is black with white inclusions, showing curviplanar and sometimes-subangular morphology.

Sample 3, collected also at Aloasí cemetery but on August 15, is dominated by: 1) a 30 % of black scoria with moderate vesicularity with spherical vesicles; 2) a 20 % of gray and reddish aggregates with subangular morphology and curviplanar surface; 3) clear-brown (cream-color) scoria which represent 20% of all particles; 4) dense fragments that correspond to andesite, subrounded or subangular in morphology, sometimes showing irregular surface mean 15% of the total; 5) free anhedral crystals of qtz are fragmented and represent 5 % of the sample; 6) reddish scoria is 5 % of the sample and their particles are moderately vesicular, subangular and with irregular surfaces. Finally, few particles correspond to volcanic glass (3%) and pumice (2 %). Pumice has blocky morphology, medium to high vesicularity and vesicles are spherical shape.

At all the cemeteries (Aloasí and Mulaló, samples 4, 5 and 6), a complex distribution of principal components was observed in the ash collected in August 23 and 24. The most abundant component is dense grey to black fragments (35-50 %), sometimes with pyrite, malaquite and white inclusions. Their morphology varies from angular to rounded and maximum clast sizes of 2 mm diameter are observed at Mulaló. Black scoria (5-40 %) show moderate vesicularity associated to spherical vesicles and blocky morphology with irregular surfaces. Free crystals (5-20 %) are commonly anhedral to subhedral qtz with tabular morphology, sometimes fractured. The px crystals are semi-planar, subangular and greenish (hypersthene?). Also, free crystals of pyrite are found. Aggregates (5-20 %) vary in color (white, grey and brown color), with angular, subrounded and in very rare cases, rounded morphologies. Volcanic glass (5-15 %) is black, with morphologies varying from angular to subrounded and their surface is brilliant, with white inclusions. The brown (or cream color) scoria fragments (5-25 %) are blocky or irregular, their vesicularity varies from low to moderate and in some cases these vesicles are filled. Largest particles reach 4 mm diameter. Reddish scoria is very infrequent (5 %), with blocky morphology and moderate to high vesicularity.

Significant variability is also observed in the ash samples collected on August 24 (from 7 to 10). Samples collected at San Ramón, Lasso, San Agustín de Callo and the Cotopaxi Nat. Park entry (samples 7, 8, 9 and 10, respectively) are characterized by abundant (20-50 %) dense fragments, which vary from gray to black color, with angular to subrounded morphologies, that show traces or presence of oxidized and magnetic minerals, respectively. At San Ramón, the largest dense fragments are 1.5 mm diameter and some of them exhibit pyrite whereas at Lasso these dense fragments correspond to andesites. Aggregates are also very common (10-50 %) and are observed in a variety of colors (eg. white, gray, orange, green) and morphologies (angular, subangular, subrounded, rounded and planar), some of them with largest sizes of 1 mm diameter at the Cotopaxi Park entry. Free crystals (15-40 %) are represented by tabular, subhedral or euhedral crystals (in some cases fractured) of qtz and subhedral greenish px crystals (hypersthene?), in some cases rounded to subangular. Volcanic glass has been only identified in the San Ramón sample, representing 5 % of the sample.

Temporal evolution of ash components is reported in Fig. 7. In general, the ash samples from the first days of eruption (1, 2 and 3) show more variability in terms of components, while at the samples from August 24 (7, 8, 9 and 10) are exclusively compound of lithics, free crystals and aggregates (Fig. 7). Between these two discrete tendencies, there are three samples (4, 5 and 6) which are likely "transitional" and show characteristics of both extremes (Fig. 7).

4.5 Texture

The glassy particles collected during the early stage of the eruption (14 and 15 August) are mainly dense, blocky-shaped with low vesicularity (Fig. 8A), with angular shape due to post-vesiculation evident fragmentation (Fig. 8B). Cracking is not common and it is marginal when observed (Fig. 8C). In some cases, inter-vesicular walls are preserved after fragmentation (Fig. 8D). Fresh juvenile textures are completely absent within this period. Textural variations are observed on the samples collected on 24 August. In fact, glassy particles are in most cases blocky-shaped with low to moderate vesicularity, while rarely non-vesicular dense particles are also observed. The blocky fragments vary from 300 to 1400 μm (~-0.5 to 1.74 Φ), in some cases they are subrounded, showing vesicle bursting (Fig. 8E), sometimes seen as peripheral vesicles (Fig. 8F). Glassy, subrounded particles with smooth surface (Fig. 8G) are noticed but scarce, with size varying from 700 to 800 μm (0.32 to 0.52 Φ). Weak vesicles can be observed over solidified bubbles freeze during their expansion, and produces a "molten surface" (Fig. 8H). The non-vesicular particles are generally irregular, and in some cases they show a "rough" surface full of pitting (Fig. 9I) . In general, the surfaces of these particles are clean of adhering particles, with minor exceptions in dense grains (Fig. 8H and 8I).

The free crystals observed on the 24 August samples are massive, dense, irregular to subrounded (Fig. 8J and 8K) and commonly conchoid-fractured, showing smooth surface and fractured edges, typically 300-800 μm in diameter.

The aggregates are present within the whole time series and correspond to massive accretionary pellets with subspherical to irregular shape (Fig. 8L to 8M), rugged surface, 20 to 40 % porosity, typically 500-700 μm (0.52 to 1.0 Φ) in diameter. Their subspherical to irregular inter-granular porosity is 30-50 μm (4.34 to 5.0 Φ) in diameter.

4.6 Geochemistry and mineralogy

Geochemical studies include the analysis of bulk ash samples or most commonly glassy particles. From 10 bulk ash geochemical XRF analyses, most of the results show high (>1.0 wt. %) material loss on ignition (LOI). Specifically, the higher LOI values (between 2.90 and 9.54 wt. %) are observed within the samples from the initial phase of the eruption (samples 1 to 3, 14-15 August), and then decrease to values lower than 2.0 wt. %. Thus, bulk ash composition is reported from samples 8 and 9 (24 August, LOI <1%). According to Le Maitre et al. (1989) classification scheme for igneous rocks, average composition for the ash is basaltic andesite (SiO_2 content of 55.67 wt. %) The ashes are compound of high average values of Al_2O_3 (17.64 wt. %), high CaO (6.99 wt. %), low TiO_2 (0.85 wt. %), low MgO (3.56 wt. %) and medium-K_2O (1.29 wt. %), as

observed in Table 3, typical for calk-alkaline magmas. From two clusters of grains suspected to be juvenile in origin (14 and 24 August), the SEM-EDS geochemical mapping yields dacitic composition (Table 3; Fig. 9), similarly to some of the particles defined as juvenile by Gaunt et al. (2016).

The ash fragments are mostly compound of pl (64.9 vol. %) and px (33.3 vol. %) (Table 4). These px are mainly clinopyroxene (cpx: 29.8 vol. %), represented by pigeonite (16.8 vol. %) and diopside (13 vol. %), and orthopyroxene (opx) which correspond to estantite (3.5 vol. %). Accessory minerals are anhydrite (1.6 vol. %) and melanterite (0.1 vol. %) and pyrite (0.1 vol. %). Analytical recognizance of anhydrite is frequently occurs within the initial stage (samples 1 to 3, 14-15 August), and pyrite is present exclusively in sample 2 (14 August).

5. Discussion

5.1 Eruption mechanism

The August 14-24 Cotopaxi volcano eruption has been ranked as VEI 2 (according to the explosivity index of Newhall and Self, 1982) and Magnitude 2.1 (based in the classification of Pyle, 2000; Bernard et al., 2016). For comparison, these values are in the same scale of magnitude with the phreatic activity of Ontake Volcano (Japan, 2014; Takarada et al., 2016).

Most of our ash samples show polymodal grain size distribution, with the exception of samples 4 and 9, which are unimodal. The presence of multiple grain size modes could be explained by different ways. First of all, different particle types show different porosity (vesicularity), which controls their fractal dimension of fragmentation at an applied potential fragmentation energy (or equivalent pressure) (Perugini and Kueppers, 2012). In our ash samples we have found from 3 to 8 particle classes, but if grain size distribution is compared with the number of particle classes, no correlation is observed. For example, samples with trimodal grain size show 6 types of particles, while other bimodal show 3, 4, 7 or 8 particle types. Another explanation could be the presence of aggregates, which have been associated to polymodal grain size distributions (e.g. Scasso et al., 1994; Durant et al., 2012). However, aggregates are always present in similar amounts during the studied period (14 to 24 August) and any correlation should not be provided with grain size distributions in this case. Despite other possible correlations, trimodal ashes are only present in the 14 August samples when activity began. We point to both highest clast variability and eruption intensity (highest eruption columns) during the initial phase of activity (explosions of August 14) as the responsible of these grain size distributions due to the ejection of country rocks of different sizes, as it has been reported for vent-cleaning Vulcanian eruptions (e.g. Clarke et al., 2015). This is supported by the coarser grain size modes found at the samples of the initial stage of the eruption (Fig. 6A to 6C). In contrast, bimodal grain size distributions observed during the subsequent days, are related to weak eruption plumes and consequently eruptions with lower intensities.

The August 14-15 Cotopaxi 2015 ash is compound of dominant dense fragments (in most of cases porphyritic lava lithics), but also of blocky scoria material, free crystals and hydrothermally altered materials, whose lithological components are similar to that

reported by Hidalgo et al. (2016) for the whole eruptive cycle. Volcanic glass is always observed in minor proportion (3-15 %) within the whole sample. These grains are dense, poorly vesiculated and highly fragmented, without any textural feature which would be attributed to magma-water interaction (i.e. well-preserved quenching cracks, stepped surfaces or mosslike pattern; Zimanowsky et al., 2015). By other hand, the higher LOI values observed in bulk ash geochemistry within the initial days of eruption, in parallel to the analytical recognizance of anhydrite and pyrite for the same period reveal an active role of the hydrothermal system during the onset of the eruption. This is in agreement with the optical recognizance of Fe and Cu minerals (e.g. pyrite and malaquite), which have been associated to crater-lake environments (e.g. Pasternack and Varekamp, 1994; Varekamp and Ouimette, 2001; Aguilera et al., 2015), hydrated sulfates such as melanterite (e.g. Hynek et al., 2013) and certainly the reddish altered scoria. Textural features such as pitting and adhering particles at dense grains analyzed under SEM is also associated to the interaction of these particles with hydrothermal fluids during eruption (Zimanowsky et al., 2015). Moreover, the finding of aggregates may be explained by hydrometeor formation (e.g. Brown et al., 2012 and references therein) or due to the formation of surface water-soluble components such as sulfate (e.g. Delemelle et al., 2007; Bagnato et al., 2013) which may cause cementation of these particles (e.g. Scolamacchia and Dingwell, 2014). This also agrees with the elevated SO_4 amount in ashes collected during September 2015, with about 1713 to 12993 mg/kg (IGEPN, 2015f). These records points to phreatic, vent-cleaning explosive style during the initial days of the eruption.

The basaltic andesitic (54.67 wt. % SiO_2) composition of bulk ash and its mineral assemblage (pl+ cpx + opx) are similar to the bulk composition of Cotopaxi products in the geological record (Fig. 9). The juvenile glassy grains identified by Gaunt et al. (2016) are almost compositionally identical to these glassy grains studied by Pistolesi (2011), specially to these deposited during the post-1880 eruptions. Our SEM-EDS geochemical mapping yields similar results to these of Gaunt et al. (2016) for juvenile grains composition. In fact, for distinguishing between non-juvenile and fresh juvenile particles, Gaunt et al. (2016) carried out petrological studies of microlite growth. Now, we report textural observations of ash particles ejected by 24 August revealing blocky-shaped glassy particles, with low to moderate vesicularity, similarly to these reported in previous studies as juvenile for phreatomagmatic eruptions using SEM observations (e.g. Heiken, 1972; Wohletz, 1983; Cas and Wright, 1987). However, glassy, blocky shaped particles and conchoidal fractures are not unique to a single process and only demonstrate that the material (melt or glass) has broken in a brittle fashion (Pardo et al., 2014). In contrast, subrounded particles with smooth surfaces as those reported here for some glassy fragments, are currently attributed to fragmentation processes within a ductile regime during the early expansion stage of magma fuel-coolant interactions (MFCI; Zimanowsky et al., 2015). According to these authors, "passive particles" are produced by stresses resulting from thermo-hydraulic explosions, in contrast to the most commonly observed phreatomagmatic fragments (or "active particles") which result from explosive, direct magma-water interactions and brittle fragmentation. In this case, the fresh juvenile glass recognition came from their crystallinity (Gaunt et al., 2016) and now from the morphology of certain passive particles. Thus, a direct magma-water interaction is unconvincing between 14-24 August from textural, geochemical and mineralogical data, and re-ejection of pyroclastic material from previous eruptions is

also a probable origin of many fresh volcanic glasses. However, some smooth, fresh glassy particles here reported on the 24 August ashes should be attributed to an indirect interaction between the volcano's hydrothermal system and a shallow, rising magmatic source.

This hypothesis is also supported by geophysical data. For instance, increase of LP and VLP seismicity prior the eruption, deep (7-11 km depth) deformation sources, increase in the magmatic signature of gas discharges (specially SO_2 and BrO) after 14 August and an increased melting of glaciers due to the warming of the volcanic edifice was yet interpreted as indubitable evidence of a magmatic intrusion by several authors (e.g. Arias et al., 2015; Dinger et al., 2016; Hidalgo et al., 2016; Mothes et al., 2016; Ramón et al., 2016). Another possible explanation for the August 2015 activity, such as the self-sealing of the hydrothermal system, is not likely due to the absence of highly altered, low permeability seal rocks, abnormally high gas ebullition and strongly CO_2 enriched gas emissions (e.g. Christenson et al., 2010). Also, these hydrothermal eruptions are commonly short lived and cyclic, currently associated to mineralization events (e.g. Browne and Lawless, 2001). Thus, the eruptive process developed by Cotopaxi between August 14 and 24, 2015 is associated to the reheating of the volcano's hydrothermal system due to a shallow, low-volume magma input, generating a initial stage of phreatic activity between 14-15 August, which evolved into a magmatic-hydrothermal eruption in the following days up to 24 August, as early suggested by Bernard et al (2016).

Our model for the current eruption has been previously explained by Fournier (1999) for economic geology purposes, attending to the formation of hydrothermal breccias and magmatic-epithermal deposits. According to our hypothesis, an new (or a series of small) magmatic input in 2015 would have transferred heat and volatiles to the brittle-plastic transition (BPT; ~400 °C isotherm, normally km 1-2 depth inside the volcano), producing the VT, LP, VLP and tremor events plus edifice deformation due to the volatile release from magmatic fluids (Fig.10A). This state should have induced a critical shear stress at the BPT, producing its fracturing and leading a sudden discharge of magmatic volatile and superheated hydrothermal fluids ("steam") within a pressure surge into the hydrostatic domain (Fig.10B). This pre-eruptive stage induced a VT earthquake swarm by rock fracturing. The pressure surges of steam are able to fragment and transport both pre-existent country rock with the subsequent formation of a phreatic, vent-cleaning phase. This is consistent with the low temperature of the eruption column (<200 °C; Bernard et al., 2016), the high amount of country rock discharged (old lavas and pyroclastic materials) and the sedimentation of ash with trimodal grain size distribution. Also, the role of "brines" was probably essential for the aggregation of particles, while the boiling of the hydrothermal system is also supported by the abundant altered rocks and the precipitation of Cu minerals as pyrite. A subsequent indirect interaction between the rising magma and the disrupted hydrothermal fluids, produced thermo-hydraulic explosions resulting in a passive fragmentation of magma, erupting these particles accompanied by residual country rock during a magmatic-hydrothermal eruptive phase between 15 and 24 August (Fig.11B). The continuation of magma ascent, may have depleted the hydrothermal system during the subsequent days, without direct evidence of phreatomagmatic fragmentation up to 24 August (Fig. 10C). This would explain the lack of "active particles" within the fresh volcanic glass during that period. Finally, the magmatic intrusion probably started

crystallizing at depth without any evidence of reaching the crater level, probably as consequence of its low volume and low ascent rates (e.g. Gaunt et al., 2016).

5.2 Ash hazards assessment

The unrest crises in 2001 and 2015 at Cotopaxi are unmistakable signatures of the active state of this volcano. Moreover, the occurrence of magmatic-hydrothermal eruptions in 2015 evidence shallow magma intrusions (e.g. Hickey et al., 2015) which can evolve into a magmatic eruption in the future, especially when the conduit of the volcano has been partially cleaned during the last eruption, and probably remains in a semi-open state (Gaunt et al., 2016). Even when small, future ash emissions or explosive events must be studied at Cotopaxi, with emphasis in the fresh juvenile magma recognition. However, ash analyses can be confusing by themselves, especially when the fresh magmatic signature is difficult to recognize following the usual techniques (grains lithology, particle morphology, glass geochemistry, etc.) or due to an elevated cost and time-consuming procedures. In fact, together with ash sampling, it is prevaling to count with a geophysical monitoring of the unrest progress to better understand its triggering factors. Due to its robust monitoring network managed by the Instituto Geofísico, Cotopaxi volcano may be well prepared for attending future unrest processes. The high-resolution geophysical background and detailed analysis of the eruptive products from multiple and autonomous research teams during this eruptive crisis offers a great learning opportunity for studying an eruptive process and for sharing knowledge, which is applicable to other volcanoes worldwide.

According to Biass and Bonadonna (2013), there is a >50 % probability of wind blowing in a west sector of Cotopaxi for altitudes between 3 and 20 km asl, and a 90 % probability of wind blowing in a sector comprised between 240° and 300° between vent level and about 13 km, and any particular trend was found during El Niño/La Niña phenomena. This is in agreement with the data of REANALYSIS for August and also with most of the trajectories of ash plumes during the August 14-24, 2015 eruptive period. Even though the respirable fraction, i.e. sub-10 □m, have not been studied in the granulometric analysis of the samples, it is important to highlight that due to the proximity of Cotopaxi volcano to Quito (~2,234,000 inhabitants) and several small towns, there is a need for the development of a protocol for rapid risk assessment, even when Quito is not a high-probability plume blowing area.

Gislasona et al. (2011) proposed a protocol after the Eyjafjallajökull eruption in 2010 that includes the evaluation of size, shape and hardness as they are key parameters for assessing the ash abrasiveness as well as the determination of the material mineral composition. Also, studies of recent eruptions also promote the ash leachate analyses in order to understand the substrate reactivity, which poses health, environmental and economic threats, especially during hydrovolcanic eruptions (e.g. Durant et al., 2012; Cronin et al., 2014). In consequence, the ash leachate analyses are highly recommended for future studies in the Cotopaxi area after the 2015 eruption. These characterizations together with the estimation of the mass of ash produced, plume height, grain size distribution, and the dispersion rate would provide input for modeling to predict the hazard level and establish an emergency civil protection protocol. Monitoring of impacts of thin ash falls (< 2 mm thickness) is not frequent (Jenkins et al. 2015). Thus, their hazards are not well understood in terms of emergency management planning and

more studies are needed in order to understand their impacts. In this context, the Cotopaxi 2015 eruption provides a good opportunity to focus on these aspects.

6. Conclusions

Cotopaxi volcano newly erupted on August 14 (2015), producing low-energy (VEI 2), locally-distributed basaltic andesitic (55.67 wt. % SiO_2) bulk ash emissions. The surface activity was preceded by an unrest period since April 2015, which consisted of increased seismicity, sulfur emissions and edifice inflation. The precursory seismic activity was larger in the number of events than the one recorded for the 2001-2002 unrest period. During the first few hours of eruption, several explosions occurred, producing ash columns of 8.7 and 13 km altitude, while their plumes were dispersed mainly toward NW, W, SW, and E-SE directions from the vent. On the following days, ash emissions were frequent but spaced in time and the columns elevated 0.2-2 km acl, with their plumes being dispersed toward the west. All these wind-blowing tendencies are in agreement with statistic values recorded at Cotopaxi area. Grain size analyses of ash samples are interpreted as a result of different eruption intensity, which is also supported by coarser grain size fractions on the initial days of eruption. The textural analyses revealed that the small amount of fresh volcanic glass found in ash by 14-15 August were brittle-fractured, highly altered and accompanied by hydrothermal minerals. Thus, we suggest that the most probable origin of this ash is the recycling of country rock triggered by a reheating of the hydrothermal system (phreatic activity). Samples of 24 August characterized by a decrease of ash alteration and the finding of fresh glassy particles associated to magmatic fragmentation within a ductile regime, thus suggest an indirect interaction between a rising magma and the hydrothermal system during magmatic-hydrothermal eruptions. Geophysical background do confirm the presence of a magmatic intrusion as the triggering factor for the August 2015 eruption, but not its arrival at surface level during the eruptive period. Similarly, we did not found any evidence of a direct interaction between rising magma and hydrothermal system producing thus phreatomagmatic activity. Laser grain size, leachate analyses and human health studies are needed for determining the impact of ash falls at Cotopaxi volcano. New protocols have to be established in order to evaluate unrest and eruption process of centennial-dormant volcanoes which develop unrest periods evolving into hydrovolcanic activity. Robust geophysical monitoring should to be accompanied by periodic real-time ash analysis at any of these volcanoes.

Acknowledgements

Laboratory (XRF, XRD and SEM) analyses were supported by the DEMEX-PII-003-2016 internal project grant at Departamento de Metalurgia Extractiva from Escuela Politécnica Nacional. We are grateful with Mr. Andrés Ordóñez by his assistance during fieldwork. The authors express their gratitude to Mr. Leif Castren for his valuable English revision and to Dr. Daniel Tormey who provided a fruitful review of the final manuscript. We appreciate the comments by Editor Dr. Joan Marti and an anonymous reviewer who greatly improved this manuscript.

References

Afpes, 2015. https://www.youtube.com/watch?v=jk7gq6LI5QM. Accessed in August 6, 2016.

Aguilera, F., Benavente, O., Gutiérrez, F., Romero, J., Saltori, O., González, R., Augusto, M., Caselli, A., Pizarro, M., 2015. Eruptive activity of Planchón Peteroa volcano for period 2010-2011, Southern Andean Volcanic Zone, Chile. Andean Geology 43 (1): 20-46.

Arias, G., Molina, C., Ruiz, M., Kumagai, H., Hernández, S., Plain, M., Mothes, P., Yepez, M., Barrington, C., Hidalgo, S., 2015. Very long period seismicity accompanying increasing shallower Activity at Cotopaxi volcano. In AGU Fall Meeting, San Francisco, 14-18 December 2015. S51D-2724.

Bagnato, E., Aiuppa, A., Bertagnini, A., Bonadonna, C., Cioni, R., Pistolesi, M., Pedone, M., Hoskuldsson, A., 2013. Scavenging of sulphur, halogens and trace metals by volcanic ash: the 2010 Eyjafjallajökull eruption. Geochimica et Cosmochimica Acta, 103, 138-160.

Barberi, F., Coltelli, M., Frullani, A., Rosi, M., Almeida, E., 1995. Chronology and dispersal characteristics of recently (last 5000 years) erupted tephra of Cotopaxi (Ecuador): implications for long-term eruptive forecasting. J. Volcanol. Geotherm. Res., 69 (3-4): 217-239.

Bernard, B., Battaglia, J., Proaño, A., Hidalgo, S., Vásconez, F., Hernandez, S., Ruiz, M., 2016. Relationship between volcanic ash fallouts and seismic tremor: quantitative assessment of the 2015 eruptive period at Cotopaxi volcano, Ecuador. Bulletin of Volcanology, 78(11), 80.

Biass, S., Bonadonna, C., 2013. A fast GIS-based risk assessment for tephra fallout: the example of Cotopaxi volcano, Ecuador. Part I: probabilistic hazard assessment. Nat. Hazards, 65:477–495.

Blott, S.J., Pye, K., 2001. Gradisat: a grain size distribution and statistics package for the analysis of unconsolidated sediments. Earth Surf. Process. Landf., 26: 1237-1248.

Bonadonna C., Costa A., 2012. Estimating the volume of tephra deposits: A new simple strategy. Geology, 40 (5): 415–418.

Brown, R.J., Bonadonna, C., Durant, J.C., 2012. A review of volcanic ash aggregation. Phys. Chem. Earth, 45–46: 65–78.

Browne, P.R.L., Lawless, J.V., 2001. Characteristics of hydrothermal eruptions, with examples from New Zealand and elsewhere. Earth-Science Reviews, 52: 299-331.

Cas, R. A. F., Wright, J. V., 1987. Volcanic Successions, Modern and Ancient: A Geological Approach to Processes, Products and Successions, 528 pp.

Cashman, K.V., Hoblitt, R.P., 2004. Magmatic precursors to the 18 May 1980 eruption of Mount St. Helens, USA. Geology, 32 (2): 141–144.

Clarke, A.B.; Ongaro, T.E.; Belousov, A.; 2015. Vulcanian eruptions. In: Sigurdsson, H., Houghton, B., McNutt, S., Rymer, H., & Stix, J. (Eds.). (2015). The Encyclopedia of Volcanoes. Elsevier.

Chancusig, E. 2015. https://www.youtube.com/watch?v=uglxoR2n_cA . Accessed in August 6, 2016.

Christenson, B. W., Reyes, A. G., Young, R., Moebis, A., Sherburn, S., Cole-Baker, J., Britten, K., 2010. Cyclic processes and factors leading to phreatic eruption events: Insights from the 25 September 2007 eruption through Ruapehu Crater Lake, New Zealand. J. Volcanol. Geotherm. Res., 191(1), 15-32

Constantinescu, R., Rouwet, D., Gottsman, J., Sandri, L., Tonini, R. 2015. Tracking volcanic unrest at Cotopaxi, Ecuador: the use of the BET_EF tool during an unrest simulation exercise. Geophysical Research Abstracts, Vol. 17, EGU2015-2251, EGU General Assembly, Vienna, 2016.

Cronin, S. J., Stewart, C., Zernack, A. V., Brenna, M., Procter, J.N., Pardo, N., Christenson, B., Wilson, T., Stewart, R.B., Irwin, M., 2014. Volcanic ash leachate compositions and assessment of health and agricultural hazards from 2012 hydrothermal eruptions, Tongariro, New Zealand. J. Volcanol. Geotherm. Res., 286: 233-247.

Dellino, P., Kyriakopoulos, K., 2003. Phreatomagmatic ash from the ongoing eruption of Etna reaching the Greek island of Cefalonia. J. Volcanol. Geotherm. Res., 126: 341-345

Dinger, F., Arellano, S., Battaglia, J., Bobrowski, N., Galle, B., Hernández, S., Hidalgo, S., Hörmann, C., Lübcke, P., Platt, U., Ruiz, M., Warnach, S., Wagner, T., Variations of the BrO/SO_2 molar ratios during the 2015 Cotopaxi eruption. Geophysical Research Abstracts Vol. 18, EGU2016-1001, EGU General Assembly, Vienna, 2016.

Durant, A. J., Villarosa, G., Rose, W. I., Delmelle, P., Prata, A. J., Viramonte, J. G., 2012. Long-range volcanic ash transport and fallout during the 2008 eruption of Chaitén Volcano, Chile. Phys. Chem. Earth, Parts A/B/C, 45: 50-64.

Folk, R.L., Ward, W.C., 1957. Brazos river bar: A study in the significance of grain size parameters. Journal of Sedimentary Petrology, 27: 3-26.

Fournier, R. O., 1999. Hydrothermal processes related to movement of fluid from plastic into brittle rock in the magmatic-epithermal environment. Economic Geology, 94(8), 1193-1211.

Gaunt, H. E., Bernard, B., Hidalgo, S., Proaño, A., Wright, H., Mothes, P., Criollo, E., Kueppers, U., 2016. Juvenile magma recognition and eruptive dynamics inferred

from the analysis of ash time series: The 2015 reawakening of Cotopaxi volcano. J. Volcanol. Geotherm. Res., 328, 134-146.

Gislasona, S.R., Hassenkamb, T., Nedelb, S., Bovetb, N., Eiriksdottira, E.S., Alfredssona, H.A., Hemb, C.P., Baloghb,Z.I., Dideriksenb, K., Oskarssona, N., Sigfussonc, B., Larsena, G., Stippb, S.L.S., 2011. Characterization of Eyjafjallajökull volcanic ash particles and a protocol for rapid risk assessment. PNAS, 108 (18): 7307-7312.

Hall, M., Mothes, P., 2008.The rhyolitic-andesitic eruptive history of Cotopaxi volcano, Ecuador. Bull. Volcanol., 70: 675-702.

Heiken, G., 1972. Morphology and petrography of volcanic ashes. GSA Bulletin, 83(7): 1961-1988.

Hickey, J., Gottsmann, J., Mothes, P., 2015. Estimating volcano deformation source parameters with a finite element inversion: The 2001-2002 unrest at Cotopaxi volcano, Ecuador. J. Geophys. Res., 120(3): 1473-1486.

Hidalgo, S., Bernard, B., Battaglia, J., Gaunt, E., Barrington, C., Andrade, D., Ramón, P., Arellano, S., Yepes, H., Proaño, A., Almeida, S., Sierra, D., Dinger, F., Kelly, P., Parra, R., Bobrownski, N., Galle, B., Almeida, M., Mothes, P., Alvarado, A., 2016. Cotopaxi volcano's unrest and eruptive activity in 2015: mild awakening after 73 years of quiescence. Geophysical Research Abstracts Vol. 18, EGU2016-5043-1, EGU General Assembly, Vienna, 2016.

Hincks, T. K., Komorowski, J. C., Sparks, S. R., Aspinall, W. P., 2014. Retrospective analysis of uncertain eruption precursors at La Soufrière volcano, Guadeloupe, 1975–77: volcanic hazard assessment using a Bayesian Belief Network approach. J. of Appl. Volcanol., 3(1), 3.

Hynek, B. M., McCollom, T. M., Marcucci, E. C., Brugman, K., Rogers, K. L. 2013. Assessment of environmental controls on acid-sulfate alteration at active volcanoes in Nicaragua: Applications to relic hydrothermal systems on Mars. J. Geophys. Res.: Planets, 118 (10): 2083-2104.

Horwell, C.J.,Baxter, P.J., 2006. The respiratory health hazards of volcanic ash: A review for volcanic risk mitigation, Bull. Volcanol., 69: 1-24.

IGEPN, 2015. Informe especial Volcán Cotopaxi.

a. N°2. Anomalías de actividad (2 de Junio de 2015)

b. N° 3. Actualización de la actividad (11 de Junio de 2015).

c. N° 5. Incremento en la actividad (14 de Agosto de 2015).

d. N° 6. Incremento en la actividad (14 de Agosto de 2015).

e. N° 9. Análisis de la actividad del volcán Cotopaxi y propuesta de escenarios (21 de Agosto de 2015).

f. N°14 Observaciones visuales y térmicas del volcán, disminución de la energía sísmica y características de las cenizas analizadas (05 de Septiembre de 2015)

Inman, D.L.,1952. Measures for describing the size distribution of sediments. J. Sediment. Res. 22:125–145

Jenkins, S.F., Wilson, T., Magill, C., Miller, V., Stewart, C., Blong, R., Marzocchi, W., Boulton, M., Bonadonna, C., Costa A., 2015. Volcanic ash fall hazard and risk. In: Global Volcanic Hazards and Risk. Eds. Loughlin, S., Sparks, S., Brown, S., Jenkins, S., and Vye-Brown, C. Cambridge University Press,173-222.

Kawabata, E., Bebbington, M.S., Cronin, S.J., Wang, T., 2013. Modeling thickness variability in tephra deposition. Bull. Volcanol. 75:738.

Lawless, J.V., White, P.J., Bogie, I., Paterson, L.A., Cartwright, A.J., 1997. Epigenetic magmatic-related mineral deposits: Exploration based on mineralization models. Unpublished lecture notes for Kingston Morrison seminars, Manila and Jakarta, September 1997.

Le Maitre, R.W., Bateman, P., Dudek, A., Keller, J., Lameyre, J., Le Bas, M. J., Sabine, P. A., Schmid, R., Sorenson, H., Streckeisen, A., Woolley, A. R. and Zanettin, B., 1989. A Classification of Igneous Rocks and a Glossary of Terms. Oxford: Blackwell, 342 p.

Magill, C., Wilson, T., Okada, T. 2013. Observations of tephra fall impacts from the 2011 Shinmoedake eruption, Japan. Earth Planets Space, 65: 677-698.

Molina, I., Kumagai, H., García-Aristizábal, A., Nakano, M., Mothes, P., 2008. Source process of very-long-period events accompanying long-period signals at Cotopaxi Volcano, Ecuador. J. Volcanol. Geotherm. Res.,176:119-133.

Mothes, P., Hall, M., Janda, R. 1998. The Enormous Chillos Valley Lahar: an ash-flow generated debris flow from Cotopaxi volcano, Ecuador. Bull. Volcanol., 59: 233-244.

Mothes, P.A., Nocquet, J-M., Yépez, M.A., Jarrín, P.A., Ruiz, M.C., Gaunt, E., 2016. Flank deformation recorded during Cotopaxi's awakening in 2015. Geophysical Research Abstracts Vol. 18, EGU2016-10142-3, EGU General Assembly, Vienna, 2016.

Newhall, C.G., Self, S., 1982. The volcanic explosivity index (VEI)-an estimate of explosive magnitude for historical volcanism. J. Geophys. Res. 87: 1231-1238.

Palma, J.L., 2013. Wind Reanalysis, https://vhub.org/resources/windre.

Pardo, N., Cronin, S.J., Németh, K., Brenna, M., Schipper, I., Breard, E., White, J.D.L., Procter, J., Stewart, B., Agustín-Flores, J., Moebis, A., Zernack, A., Kereszturi, G., Lube, G., Auer, A., Neall, V., Wallace, C., 2014. Perils in distinguishing phreatic from phreatomagmatic ash; insights into the eruption mechanisms of the 6 August

2012 Mt. Tongariro eruption, New Zealand. J. Volcanol. Geotherm. Res., 286: 397-414.

Paredes, P. 2015. https://www.youtube.com/watch?v=sJiHqOmdmx4. Accessed in August 6, 2016.

Pasternack, G.B., Varekamp, J.C., 1994. The geochemistry of the Keli Mutu crater lakes, Flores, Indonesia. Geochemical Journal, 28: 243-262.

Perugini, D., Kueppers, U., 2012. Fractal Analysis of Experimentally Generated Pyroclasts: A Tool for Volcanic Hazard Assessment. Acta Geophysica, 60 (3): 682-698.

Pyle, D. M., 2000. Sizes of Volcanic Eruption. Encyclopedia of Volcanoes. Academy Press. Part II, pp 263-269. San Diego California.

Pistolesi, M., 2008. Historical analysis and stratigraphy of the post-XII century pyroclastic activity at Cotopaxi volcano, Ecuador. Implication for lahar hazard assessment. Plinius, 34: 131-138.

Pistolesi, M., Rosi, M., Cioni, R., Cashman, K. V., Rossotti, A., Aguilera, E., 2011. Physical volcanology of the post–twelfth-century activity at Cotopaxi volcano, Ecuador: Behavior of an andesitic central volcano, GSA Bulletin, 123(5-6): 1193-1215.

Ramón, P., Vallejo, S., Almeida, M., Gómez, J.P., Cáceres, B., 2016. Increased melting of glaciers during Cotopaxi awakening in 2015. Geophysical Research Abstracts Vol. 18, EGU2016-10769-1, EGU General Assembly, Vienna, 2016.

Robertson, J., Thomas, C. J., Caddy, B., Lewis, A. J., 1984. Particle size analysis of soils—a comparison of dry and wet sieving techniques. Forensic Science International, 24(3), 209-217.

Ruiz, M., Guiller, B., Chatelain, J-L., Yepes, H., Hall, M., Ramón, P., 1998. Possible causes for the seismic activity observed in Cotopaxi volcano, Ecuador. Geophys. Res. Lett., 25 (13): 2305-23-08.

Scasso, R.A., Corbella, H., Tiberi, P., 1994. Sedimentological analysis of the tephra from the 12-15 August 1991 eruption of Hudson volcano. Bull. Volcanol., 56: 121-132.

Scolamacchia, T., Dingwell, D. B., 2014. Sulfur as a binding agent of aggregates in explosive eruptions. Bull. Volcanol., 76(10), 871.

Takarada, S., Oikawa, T., Furukawa, R., Hoshizumi, H., Itoh, J. I., Geshi, N., Miyagi, I., 2016. Estimation of total discharged mass from the phreatic eruption of Ontake Volcano, central Japan, on September 27, 2014. Earth, Planets and Space, 68(1): 138.

Tvcolor36, 2015. https://www.youtube.com/watch?v=JVprjGkeIdc. Accessed in August 6, 2016.

Vaca, A., Arroyo, C., Debut, A., Toulkeridis, T., Cumbal, L., Mato, F., Cruz D' Howitt, M., Aguilera, E., 2016. Characterization of fine-grained material ejected by the Cotopaxi volcano employing X-Ray Diffraction and Electron Diffraction Scattering techniques. Biol. Med. (Aligarh), 8:3.

Varekamp, J., Ouimette, A., 2001. Crater lake brines as modern analogs of ore-transporting fluids. In Geological Society of America (GSA), Annual Meeting 33 (6): p. 359. Boston.

Wilson, T.M., Stewart, C., Sword-Daniels, V., Leonard, G.S., Johnston, D.M., Cole, J.W., Wardman, J.B., Wilson, G., Bernard, S., 2012. Volcanic ash impacts on critical infrastructure, Phys. Chem. Earth, 45-46: 5-23.

Wohletz, K.H., 1983. Mechanisms of hydrovolcanic pyroclasts formation. Size, scanning electron microscopy, and experimental studies. In: Explosive Volcanism (M.F. Sherdian and F. Barbieri, Eds) J. Volcanol. Geotherm. Res., 17: 31-63.

Wolf, T., 1878. Memoria Sobre el Cotopaxi y su última Erupción Acaecida el 26 de Junio de 1877, Guayaquil, Imprenta de El Comercio, 48 p.

Zimanowski, B., Büttner, R., Dellino, P., White, D.L., Wohletz, K.H., 2015. Magma-water interaction and Phreatomagmatic Fragmentation. In: Sigurdsson, H. (Ed.). The Encyclopedia of Volcanoes (2nd. Ed.), Elsevier, Amsterdam, pp. 473-484

Figure and table captions

Fig.1: Location of Cotopaxi volcano. **A**: General elevation map of the Ecuadorian Andes in the adjacent area of Quito, including Cotopaxi volcano **B**: Detailed map of the studied area. Data measurements and ash collection points are represented by blue stars, and their labels are mentioned in Table 1. Isomass (g/m2; Bernard et al., 2016) of the total Cotopaxi 2015 tephra fall is represented by dashed lines. Base map from GeoMapApp 3.6.0 with elevation map from the Aster Volcano Archive from NASA (https://ava.jpl.nasa.gov/list.php).

Fig. 2: A: General view of the eruptive activity of Cotopaxi volcano seen from the NW on 18 August 2015. **B**: Air pollution caused by ash fallout in the town of San Agustín de Callo (SAC in Fig. 1B) by 24 August 2014.

Fig.5: Plume dispersion during the Cotopaxi 2015 eruption (between August 14 and 24) as seen by remote sensing. **A**: Eruption plume during the first explosion on 14 August, and its expansion after ca. 2 hours (**B**). **C**: Eruption plume during the second explosion on August 14, and its expansion after ca.1 (**D**). The source of pictures **A**, **B**, **C** and **D** is GOES-13 satellite imagery. **E**: Ash plume and its ash deposits as seen by ASTER satellite image during August 22.

Fig. 3: Field observations of the ash fall deposits between 14 and 24 August 2015 around Cotopaxi volcano. Labels of sampling sites are reported in Table 1.

Fig. 4: Wind rose diagrams of at Cotopaxi volcano. **A**: Reanalysis data for August between 1999 and 2011 at different altitude (7, 10 and 15 km asl). **B**: Ash dispersal between 14 and 24 August.

Fig. 6: Grain size distribution of nine samples. **A** Sample 1 (August 14, Machachi). **B** Sample 2 (August 14, Aloasí). **C** Sample 3 (August 15, Aloasí). **D** Sample 4 (August 24, Aloasí). **E** Sample 6 (August 24, Mulaló). **F** Sample 7 (August 24, San Ramón). **G** Sample 8 (August 24, San Agustin de Callo). **H** Sample 9 (24 August, Lasso). **I** Sample 10 (August 24, Cotopaxi Nat. Park.

Fig. 7: Abundance (modal %) of each clast type from ash samples collected from August 14 to 24 2015 at Cotopaxi eruption. Further information on samples is provided in Table 1.

Fig. 8: SEM images of the particle types and their morphological features. Labels from **A** to **D** show blocky-type dense particles collected between August 14 and 15. From **E** to **I**, moderately vesicular blocky-type clasts collected on 24 August are shown. These include a rare, subrounded dense fragment found at Mulaló (**G**), a dense clast with molten surface found at Aloasi (**H**) and an angular fragment with surface pitting (**I**). Free crystals are in **J** and **K** (San Ramón and Lasso, respectively). **L** and **M** show aggregates found at Aloasi, 15 August.

Fig. 9: Total alkali-silica diagram (TAS) after Le Maitre (1989). The green and orange fields correspond to SEM-EDS glass geochemical compositions reported by Pistolesi et al. (2011) for older units of Cotopaxi. Also, the pink field corresponds to bulk rock compositions reported by Barberi et al. (1995) and Pistolesi et al. (2011).

Circles are from the 2015 eruption of Cotopaxi, as reported by Gaunt et al. (2016) for glassy clasts and data from this paper (Table 3).

Fig. 10: Cartoon showing the eruption mechanism of Cotopaxi volcano between 14 and 24 August 2015. **A** shows the pre-eruptive stage of activity before 14 August, with the intrusion of magma below the BPT releasing volatiles and causing a series of geophysical precursory signals as seismicity (VT, LP and VLP) and edifice deformation. **B** Onset of the 14 August due to the breaching of the BPT (associated to a VT swarm), inducing a series of phreatic, vent-cleaning explosions. **C** By 24 August the rising of the magmatic intrusion has partially depleted the hydrothermal fluids and an indirect interaction with magma causes a magmatic-hydrothermal interaction with passive fragmentation of juvenile material.

Table 1: Location and date of data measuring and sampling. All the UTM points are WGS84 and correspond to the 17 M zone.

Table 2: Grain size parameters of Folk and Ward (1957) for 9 samples sieved mechanically (Φ units). For sample distribution, we define as U: Unimodal; B: Bimodal and T: Trimodal. In terms of sorting, the label meaning is defined as follows: PS: poorly sorted, MS: moderately sorted; WS: Well sorted; MWS: Moderately well sorted and VWS: Very well sorted.

Table 3: Geochemical composition of the 2015 Cotopaxi tephra.

*Major element abundance (wt. %) of bulk ash obtained by XRF analyses. Sample labels are associated to these of Table 1.

** Possible juvenile glassy grains, separated and analyzed by SEM-EDS.

*** Unnormalized totals

Table 4: Modal abundance (vol. %) of minerals in ash from the Cotopaxi August 14-24 2015 eruption. Sample labels are associated to these of Table 1.

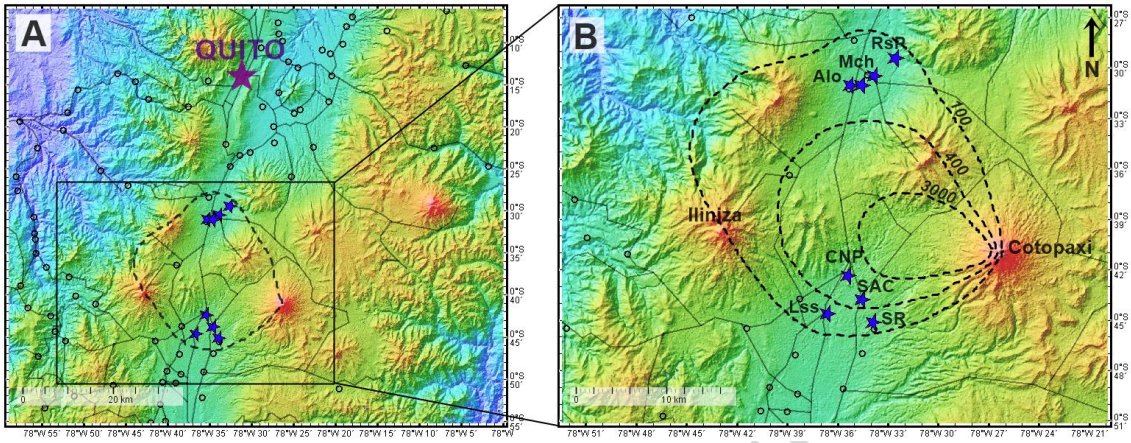

Fig. 1

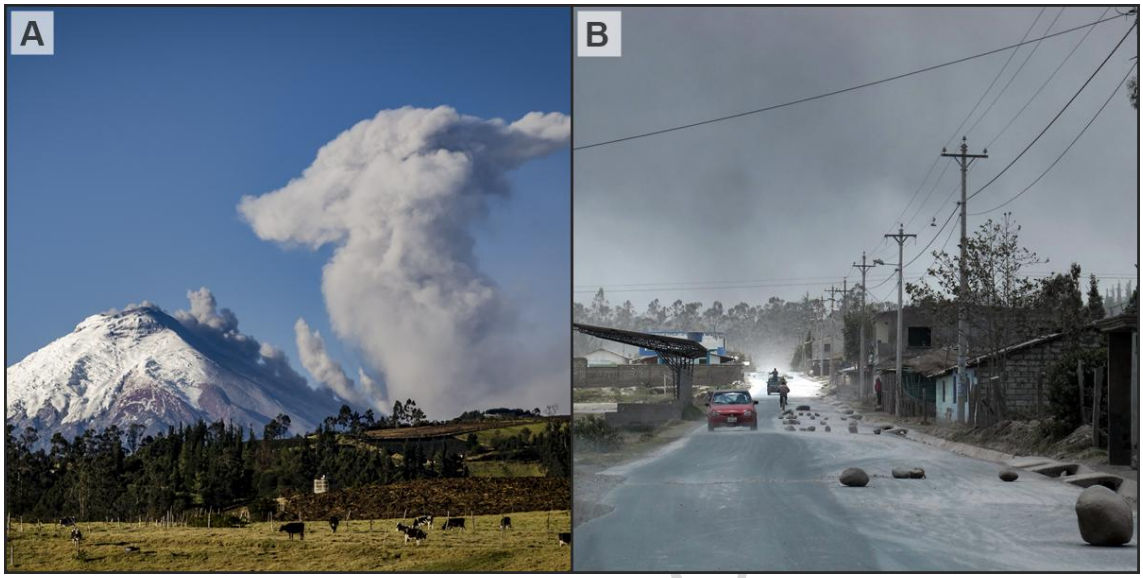

Fig. 2

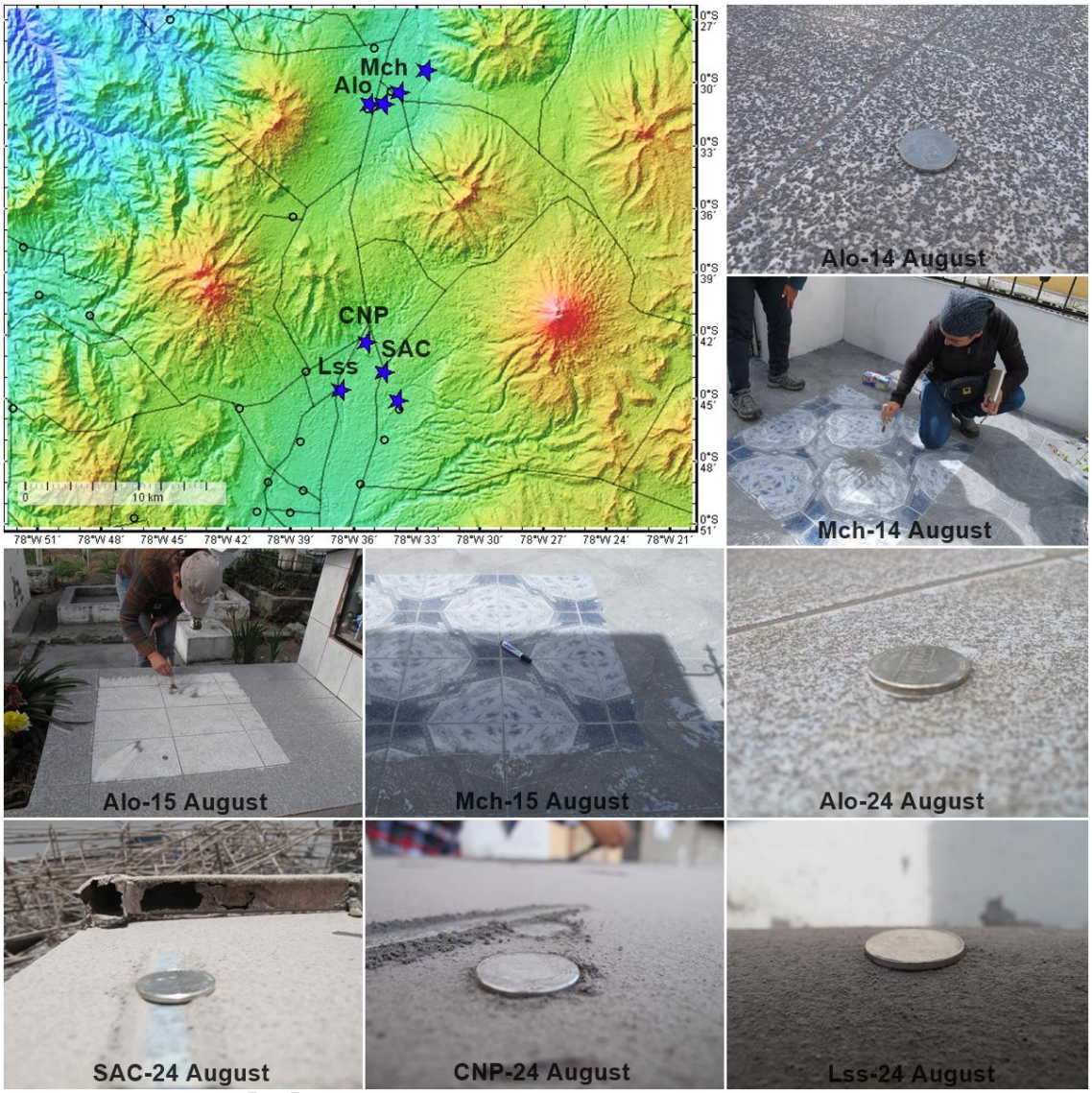

Fig. 3

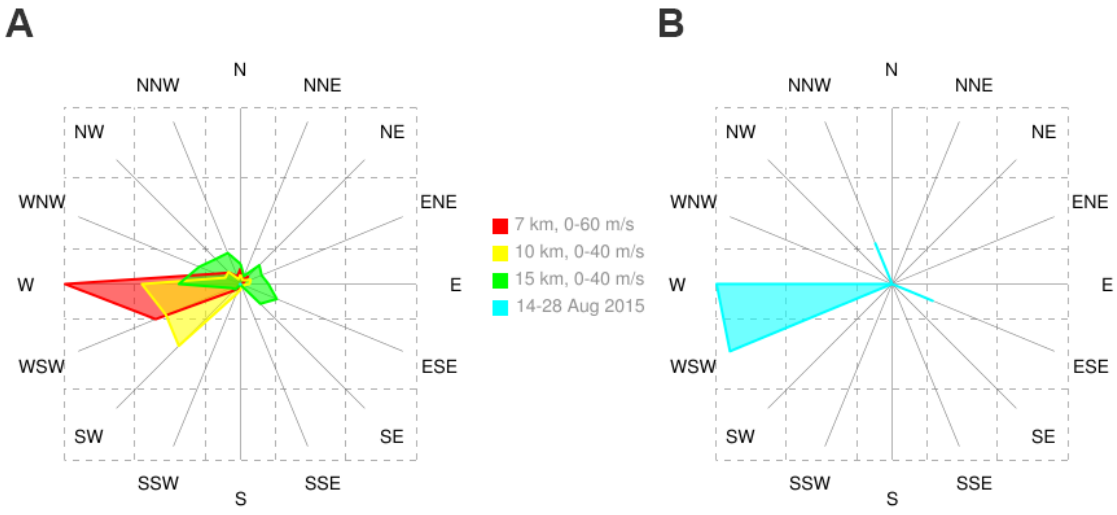

Fig. 4

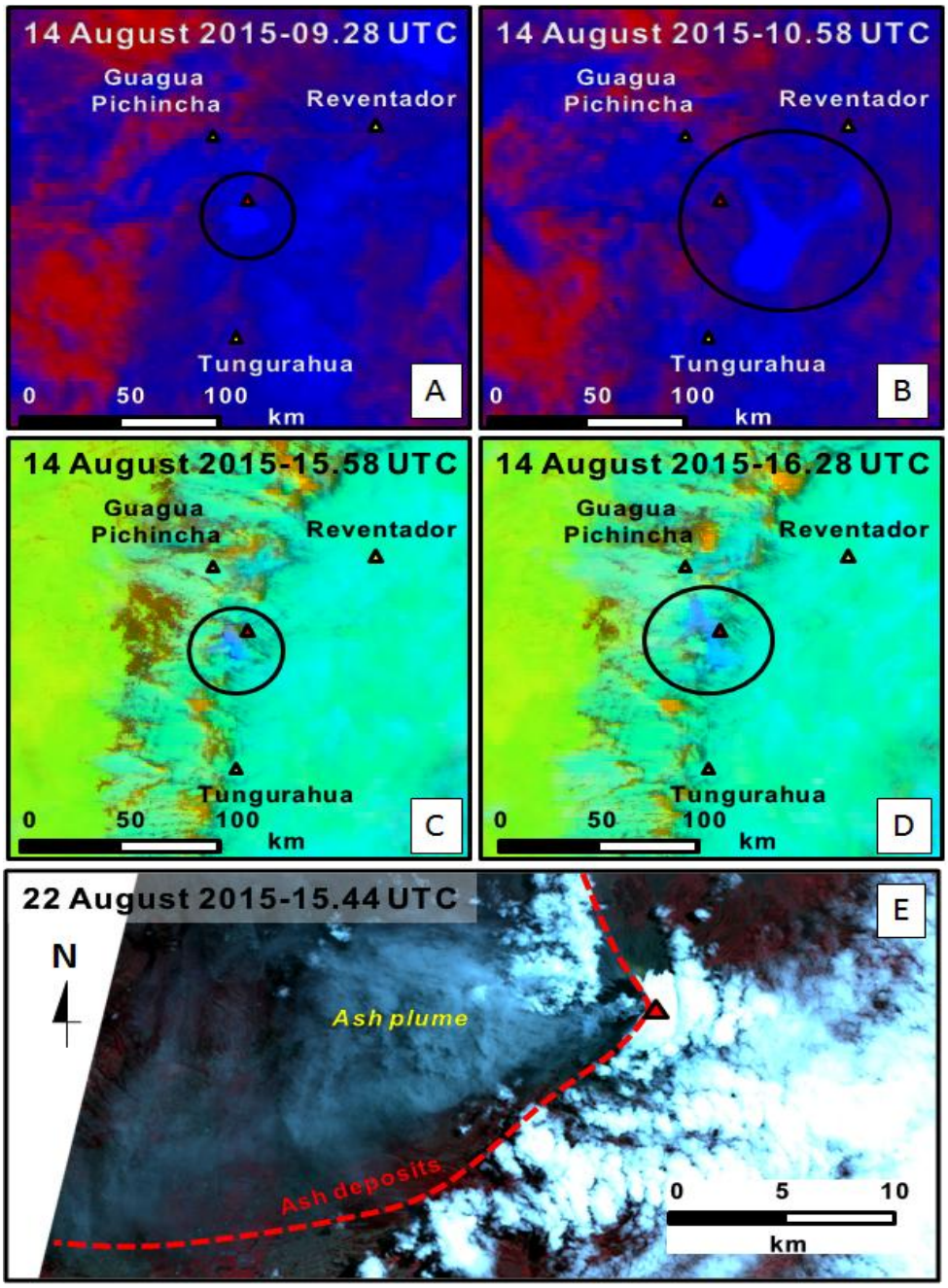

Fig. 5

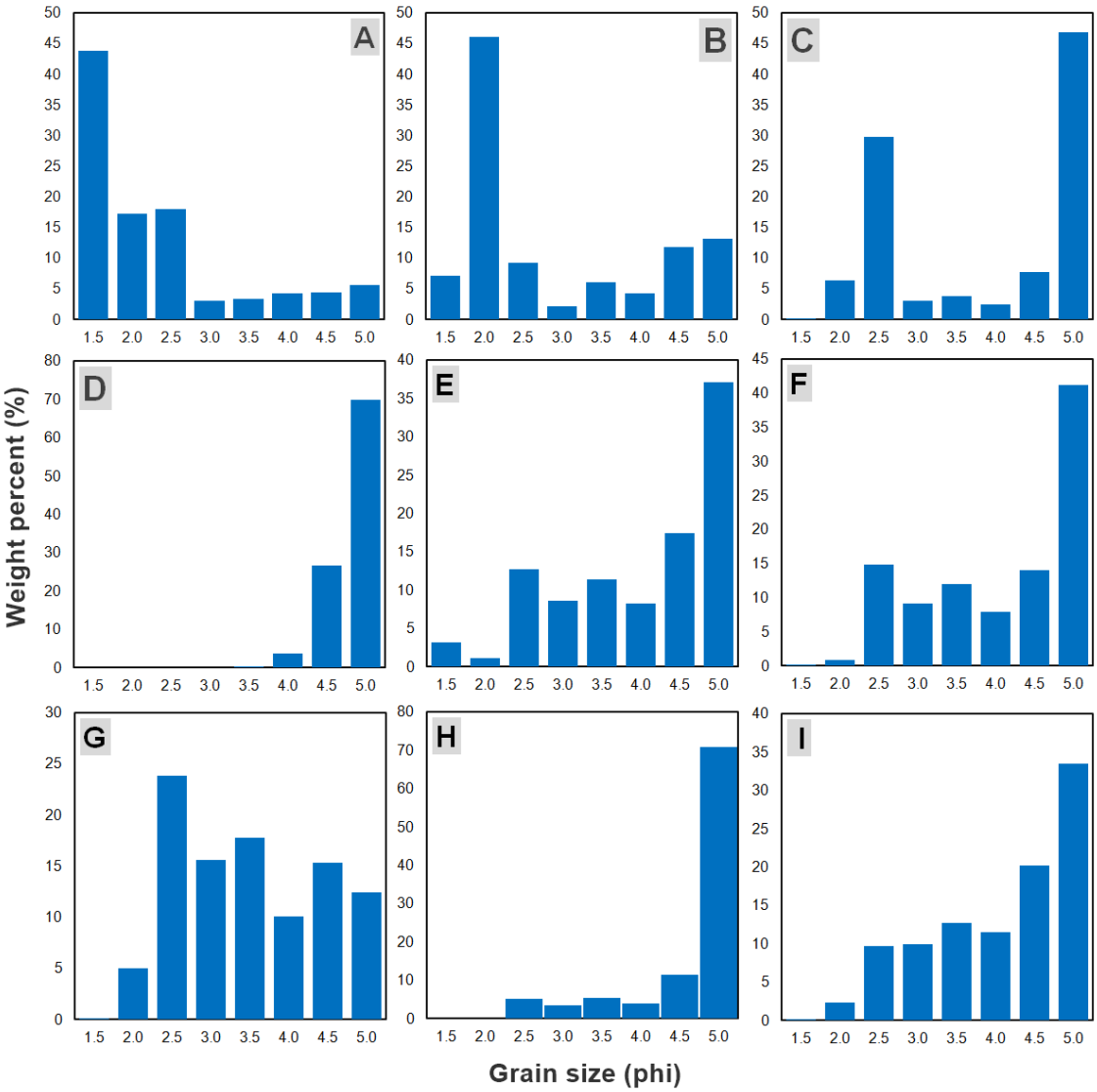

Fig. 6

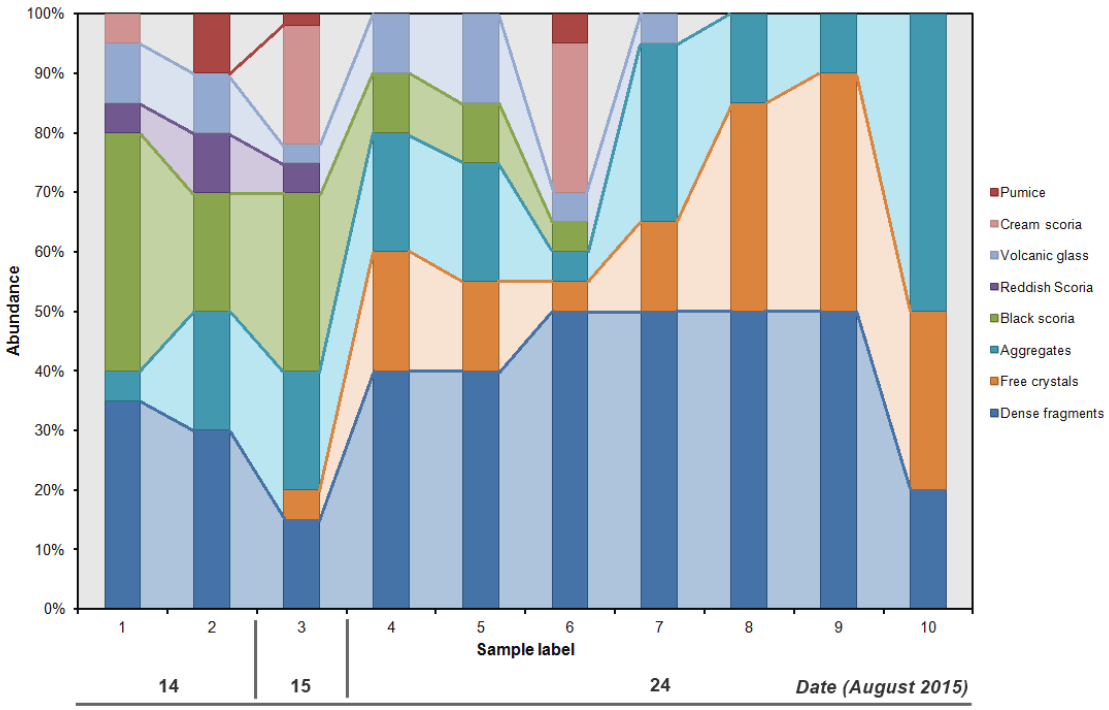

Fig. 7

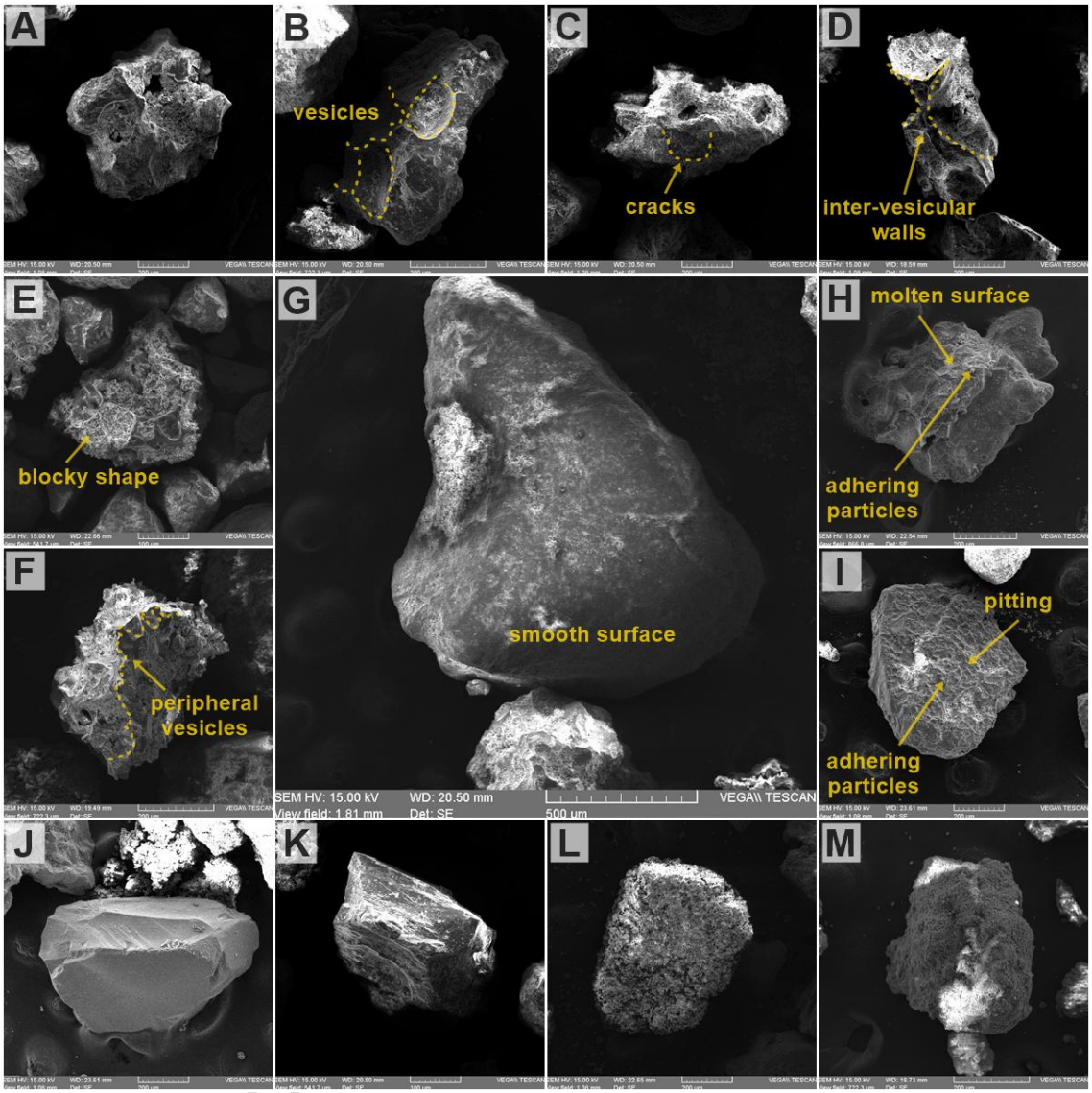

Fig. 8

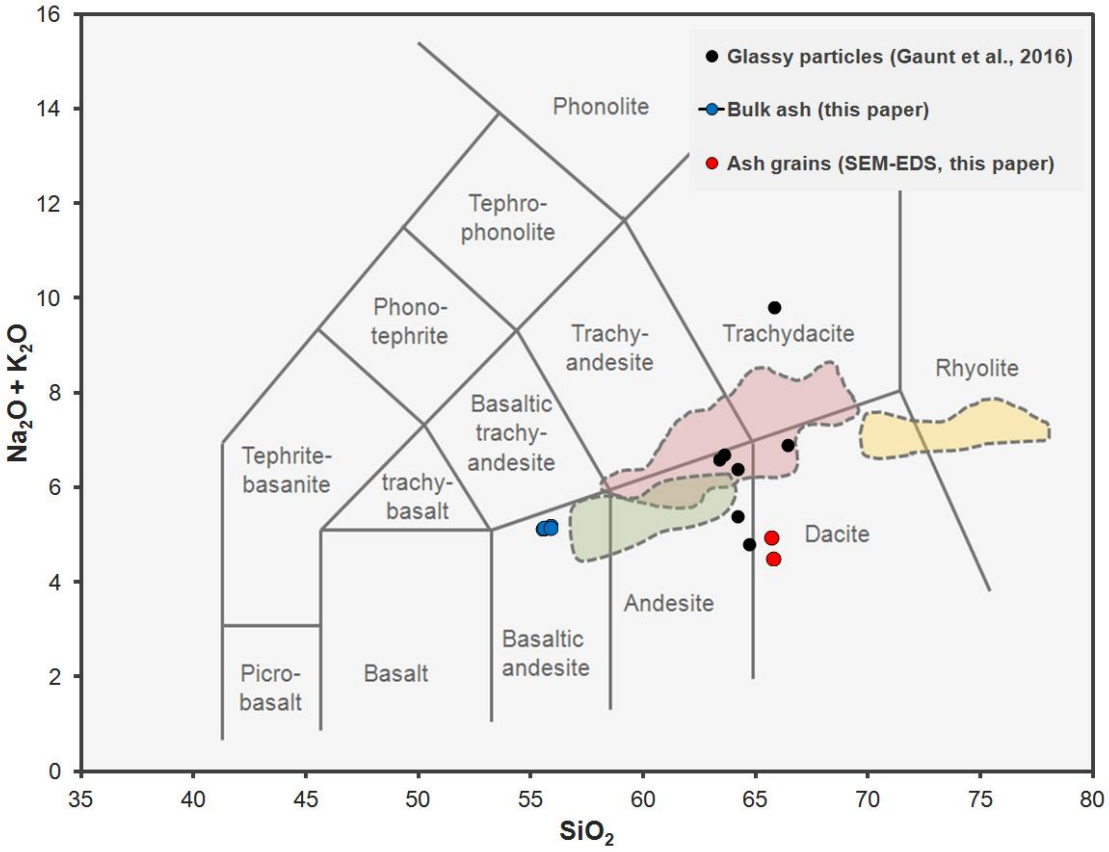

Fig. 9

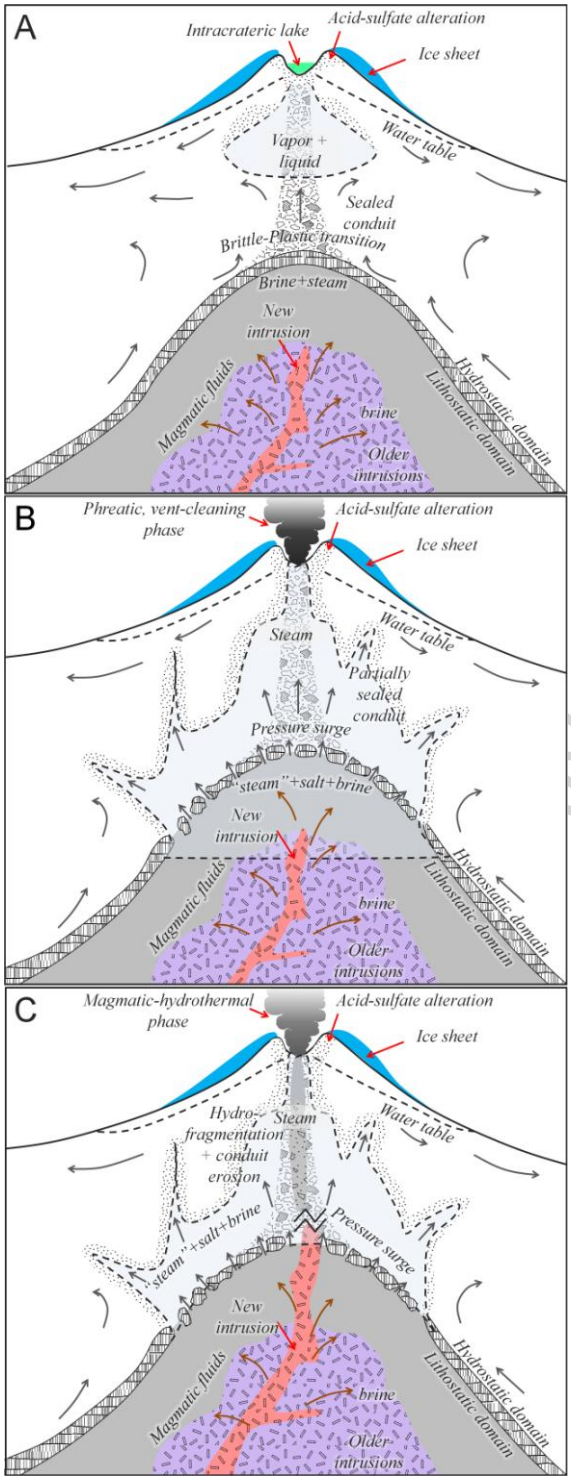

Fig. 10

Table 1

Label	Date	Easting [m]	Northing [m]	Location	Sample label	Area m^2	Mass [kg]	Thickness [mm]	Bulk Density [g/m^3]
Mch	14-08-2015	771186	9943796	Machachi	1	1	0.134	1	134.0
Alo	14-08-2015	768527	9942794	Aloasí	2	0.504	0.056	1	111.0
Mch	14-08-2015	770390	9942946	Machachi	1			1.5	
RsP	14-08-2015	773526	9945746	Río San Pedro				0.5	
Mch	15-08-2015	771186	9943796	Machachi		1	0.003	0.5	5.9
Alo	15-08-2015	768527	9942794	Aloasí	3	1	0.007	0.5	14.3
Alo	24-08-2015	768524	9942798	Aloasí	4, 5			0.5	
Mul	24-08-2015	769776	9914228	Mulaló	6			0.5	
SR	24-08-2015	771022	9916766	San Ramón	7			1	
SAC	24-08-2015	769791	9919260	San Agustín de Callo	8			2	
Lss	24-08-2015	765960	9917692	Lasso	9			1	
CNP	24-08-2015	768273	9921874	Cotopaxi Nat. Park (Entry)	10			2.5	

Table 2

Description	Sample label								
	1	**2**	**3**	**4**	**6**	**7**	**8**	**10**	**9**
	T, PS	T, PS	B, MS	U, VWS	B, MWS	B, MWS	B, MWS	B, MWS	U, WS
	Parameter								
Mean, M_z	1.61	2.32	3.19	3.74	3.23	3.26	2.89	3.26	3.62
Sorting, σ_1	1.16	1.02	0.76	0.22	0.65	0.63	0.64	0.60	0.43
Skewness, S_k	0.19	0.39	-0.58	-0.50	-0.34	-0.37	0.14	-0.24	-0.74
Kurtosis, K_G	0.89	0.73	0.56	1.12	0.72	0.68	0.83	0.75	1.79
	Modes								
Mode 1	2.24	1.62	3.86	3.86	3.86	3.86	2.87	3.86	3.86
Mode 2	3.86	3.86	2.24		2.87	2.87	3.86	3.12	
Mode 3	3.12	2.87							

Table 3

	Sample label*									Date**	
Oxide	**1**	**2**	**3**	**4**	**6**	**7**	**8**	**9**	**10**	**14-ago**	**15-ago**
SiO_2	52.3	51.79	54.94	55.85	55.32	55.99	55.5	55.85	55.56	65.8	65.67
Al_2O_3	15.29	15.25	16.91	17.71	17.22	17.35	17.5	17.77	17.71	14.52	16.04
Fe_2O_3	6.95	7.04	7.79	7.57	7.54	7.78	7.7	7.67	7.56	7.59	7.16
CaO	6.22	6.22	7.03	7.03	6.83	6.85	6.93	7.05	7.08	4.74	4.7
Na_2O	3.06	3.09	3.61	3.85	3.79	3.81	3.85	3.9	3.85	2.98	3.31
MgO	2.52	2.58	3.21	3.42	3.5	3.79	3.65	3.47	3.42	1.6	1.84
K_2O	1.14	1.14	1.23	1.3	1.27	1.27	1.29	1.29	1.3	1.53	1.64
TiO_2	0.81	0.81	0.83	0.84	0.83	0.85	0.85	0.84	0.85	0.87	0.68
SO_3	1.87	1.8	1.55	0.79	0.85	0.69	0.74	0.82	0.97	0	0
P_2O_5	0.21	0.21	0.23	0.22	0.22	0.22	0.23	0.23	0.23	0	0
Mn_2O_3	0.1	0.1	0.14	0.16	0.16	0.17	0.17	0.16	0.16		
LOI	9.48	9.54	2.9	1.06	1.89	1.22	0.92	0.87	1.13	--	--
Total* **	99.95	99.57	100.37	99.8	99.42	99.99	99.33	99.92	99.82	99.64	101.03

Table 4

		Sample label									
Mineral	**Formula**	**1**	**2**	**3**	**4**	**5**	**6**	**7**	**8**	**9**	**10**
Plagioclase	(Na, Ca)Al(Si, Al)Si_2O_8	60	63	60	68	66	68	65	66	66	67
Estantite	$Mg_2Si_2O_6$	3	3	4	5	3	2	4	4	4	3
Pigeonite	(Mg, Fe, Ca)(Mg, Fe)Si_2O_6	19	15	8	15	16	18	20	18	20	19
Diopside	$CaMgSi_2O_6$	14	13	25	12	12	12	11	11	10	10
Anhydrite	$CaSO_4$	4	4	3	0	3	0	0	1	0	1
Melanterite	$FeSO_47H_2O$	0	1	0	0	0	0	0	0	0	0
Pirite (?)	FeS_2	0	1	0	0	0	0	0	0	0	0
Total		100	100	100	100	100	100	100	100	100	100

Highlights of the manuscript:

- Ash analyses on the explosive volcanic activity of Cotopaxi between 14 and 24 August 2015
- Ash grain size, distribution, volume, geochemistry and mineralogy
- Eruption starting with phreatic style, then evolving into magmatic-hydrothermal activity with indirect magma-water interaction
- Magmatic signature in ash interpreted from passive, fresh juvenile particles